Research Article | Vol. 26, No. 16 | 6 Aug 2018 | OPTICS EXPRESS 19845
Optics EXPRESS

Realization of true all-optical AND logic gate based on nonlinear coupled air-hole type photonic crystal waveguides

VAKHTANG JANDIERI,[1,*] RAMAZ KHOMERIKI,[2] AND DANIEL ERNI[1]

[1] *General and Theoretical Electrical Engineering (ATE), Faculty of Engineering, University of Duisburg-Essen, and CENIDE - Center for Nanointegration Duisburg-Essen, D-47048 Duisburg, Germany*
[2] *Physics Department, Javakhishvili Tbilisi State University, Chavchavadze 3, 0128 Tbilisi, Georgia*
[*] *vakhtang.jandieri@uni-due.de*

Abstract: In this manuscript we propose an easily scalable true all-optical AND logic gate for pulsed signal operation based on band-gap transmission within nonlinear realistic air-hole type coupled photonic crystal waveguides (C-PCW). We call it "true" all-optical AND logic gate, because all AND gate topologies operate with temporal solitons that maintain a stable pulse envelope during the optical signal processing along the different C-PCW modules yielding ultrafast full-optical digital signal processing. We directly use the registered (output) signal pulse as new input signal between multiple concatenated nonlinear C-PCW modules (i.e. AND gates) to setup a multiple-input true all-optical AND logic gate. Extensive full-wave computational electromagnetic analysis proves the correctness of our theoretical studies and the proposed operation principle of the multiple-input AND logic gate is vividly demonstrated for realistic C-PCWs.

OCIS codes: (230.7370) Waveguides; (230.5298) Photonic crystals; (290.5825) Scattering theory; (260.2110) Electromagnetic optics.

References and links

1. E. Yablonovitch, "Inhibited spontaneous emission in solid-state physics and electronics," Phys. Rev. Lett. **58**, 2059 (1987).
2. K. Yasumoto ed., *Electromagnetic Theory and Applications for Photonic Crystals* (CRC Press, 2005).
3. J.-M. Brosi, C. Koos, L. C. Andreani, M. Waldow, J. Leuthold, and W. Freude, "High-speed low-voltage electro-optic modulator with a polymer-infiltrated silicon photonic crystal waveguide," Opt. Express **16**, 4177–4191 (2008).
4. Y. Ishizaka, Y. Kawaguchi, K. Saitoh and M. Koshiba, "Design of ultra compact all-optical XOR and ANG logic gates with low power consumption," Opt. Commun. **284**, 3528–3533 (2011).
5. P. Rani, S. Fatima, Y. Kalra and R. K. Sinha, "Realization of all optical logic gates using universal NAND gates on photonic crystal platform," Superlatt. Microstruct. **109**, 619–625 (2017).
6. P. Andalib and N. Granpayeh, "All-optical ultracompact photonic crystal AND gate based on nonlinear ring resonators," J. Opt. Soc. Am. B **26**, 10–16 (2009).
7. P. Andalib and N. Granpayeh, "All-optical ultracompact photonic crystal NOR gate based on nonlinear ring resonators," J. Opt. A: Pure Appl. Opt. **11**, 085203 (2009).
8. Y. Fu, X. Hu and Q. Gong, "Silicon photonic crystal all-optical logic gates," Phys. Lett. A **377**, 329–333 (2013).
9. C. Husko, T. D. Vo, B. Corcoran, J. Li, T. Krauss and B. Eggleton, "Ultracompact all-optical XOR logic gate in a slow-light silicon photonic crystal waveguide," Opt. Express **19**, 20681–20690 (2011).
10. Q. Liu, Z. Ouyang, C. Wu, C. Liu and J. Wang, "All-optical half adder based on cross structures in two-dimensional photonic crystals," Opt. Express **16**, 18992–19000 (2008).
11. F. Geniet and J. Leon, "Energy transmission in the forbidden band gap of a nonlinear chain," Phys. Rev. Lett. **89**, 134102 (2002).
12. R. Khomeriki, "Nonlinear bandgap transmission in optical waveguide arrays," Phys. Rev. Lett. **92**, 063905 (2004).
13. F. Wang, Z. Gong, X. Hu, X. Yang, H. Yang and Q. Gong, "Nanoscale on-chip all-optical logic parity checker in integrated plasmonic circuits in optical communication range," Sci. Rep. **6**, 24433 (2016).
14. M. Qiu, K. Azizi, A. Karlsson, M. Swillo and B. Jaskorzynska, "Numerical studies of mode gaps and coupling efficiency for line-defect waveguides in two-dimensional photonic crystals," Phys. Rev. B **64**, 155113 (2001).
15. C. Monat, B. Corcoran, D. Pudo, M. Ebnali-Heidari, C. Grillet, M. Pelusi, D. Moss, B. Eggleton, T. White and T. Krauss, "Slow light enhanced nonlinear optics in silicon photonic crystal waveguides," IEEE J. Sel. Top. Quantum Electron. **16**, 344–356 (2010).

#334971 https://doi.org/10.1364/OE.26.019845
Journal © 2018 Received 13 Jun 2018; accepted 21 Jun 2018; published 24 Jul 2018

Optics EXPRESS

16. A. Blanco-Redondo, C. Husko, D. Eades, Y. Zhang, J. Li, T. Krauss and B. Eggleton, "Observation of soliton compression in silicon photonic crystals," Nat. Commun. **5**, 3160 (2014).
17. N. N. Akhmediev and A. Ankiewicz, Solitons: *Nonlinear Pulses and Beams* (Chapman and Hall, 1997).
18. T. Krauss, "Slow light in photonic crystal waveguides," J. Phys. D: Appl. Phys. **40**, 2666 (2007).
19. R. Khomeriki, J. Leon, "All-optical amplification in metallic subwavelength linear waveguides," Phys. Rev. A **87**, 053806 (2013).
20. V. Jandieri and R. Khomeriki, "Linear amplification of optical signal in coupled photonic crystal waveguides," IEEE Photon. Technol. Lett. **27**, 639–641 (2015).
21. V. Jandieri, R. Khomeriki, D. Erni and W. C. Chew, "Realization of All-Optical Digital Amplification in Coupled Nonlinear Photonic Crystal Waveguides," Prog. Electromagn. Res. **158**, 63–72 (2017).
22. J. Leuthold, C. Koos, W. Freude, "Nonlinear silicon photonics," Nat. Photonics **4**, 535–544 (2010).
23. C. Lacava, M. A. Ettabib, P. Petropoulos, "Nonlinear silicon photonic signal processing devices for future optical networks," Apl. Sci. **7**, 103–107 (2017).
24. Y. Liu, F. Qin, Z. Meng, F. Zhou, Q. Mao and Z. Li, "All-optial logic gates based on two-dimensional low-refractive-index nonlinear photonic crystal slabs," Opt. Express **19**, 1945–1953 (2011)
25. Y. Tanaka, H. Nakamura, Y. Sugimoto, N. Ikeda, K. Asakawa and K. Inoue, "Coupling properties in a 2-D photonic crystal slab directional coupler with a triangular lattice of air holes," IEEE J. Quantum Electron. **41**, 76–84 (2005).
26. P. Strasser, R. Fluckiger, R. Wuest, F. Robin and H. Jackel, "InP-based compact photonic crystal directional coupler with large operation range," Opt. Express **15**, 8472–8478 (2007).
27. K. Yasumoto, H. Toyama and T. Kushta, "Accurate analysis of two-dimensional electromagnetic scattering from multilayered periodic arrays of circular cylinders using lattice sums technique," IEEE Trans. Anten. Propag. **52**, 2603–2611 (2004).
28. V. Jandieri, K. Yasumoto and B. Gupta, "Directivity of radiation from a localized source coupled to electromagnetic crystals," J Infra. Millim. THz Waves **30** 1102–1112 (2009).
29. V. Jandieri and K. Yasumoto, "Electromagnetic Scattering by Layered Cylindrical Arrays of Circular Rods," IEEE Trans. Anten. Propag. **59**, 2437–2441 (2011).
30. R. Khomeriki, L. Chotorlishvili, B. Malomed, J. Berakdar, "Creation and amplification of electromagnon solitons by electric field in nanostructured multiferroics," Phys. Rev. B. **91**, 041408(R) (2015).
31. M. Malishava, R. Khomeriki, "All-Phononic digital transistor on the basis of gap-soliton dynamics in an anharmonic oscillator ladder," Phys. Rev. Lett. **115**, 104301 (2015).
32. A. Taflove, *Computational Electrodynamics: The Finite-Difference Time-Domain Method*, (Artech House, (1995).
33. R. Kappeler, *Reducing the propagation losses of slab photonic crystal waveguides for active photonic devices*. Diss. ETH Zurich, No. 20485, Zurich, July 13, 2012.

1. Introduction

Photonic crystals (PhCs) have inspired a lot of interest due to their wide application for controlling light within small length scales [1, 2]. Due to their dispersion engineering features PhCs have enabled the implementation of linear functionalities into ultra-compact photonic devices. However, for the realization of true all-optical signal processing, the optical system needs to have nonlinear properties. Nonlinear PhCs are one of the most promising candidates to enable dense full-optical signal processing on the same chip leading to much lower production and operating costs even if they have to compete with ultra-compact state-of-the art optoelectronics counterparts such as e.g high-speed PhC electro-optic modulator schemes [3]. When a linear defect is introduced into the PhC, a photonic crystal waveguide (PCW) is formed and the electromagnetic wave, whose frequency lies in the band-gap region can be guided along the defect channel. If two or three PCWs are placed in a close proximity, a coupled PCW (C-PCW) is formed and the optical power is efficiently transferred from one PCW to another [2].

All-optical logic gates, which can fulfill various logical functions operations and capable of performing complex light control in all-optical circuits, have received much attention for their potential application in ultrafast information processing and optical computing systems. Various PhC structures have already been proposed to realize all-optical logic gates [4–10]. The most PhC-based logic gates rely either on resonator cavities with finite filling time or branching structures with a very confined interaction volume that is both highly sensitive to production variations and in need of pre-defines input signal phases. In this regard, the proposed formulation is advantageous due to the travelling-wave nature of the band-gap transmission, namely the resulting nonlinear traveling-wave interaction. Moreover, it is very important to mention that

Optics EXPRESS

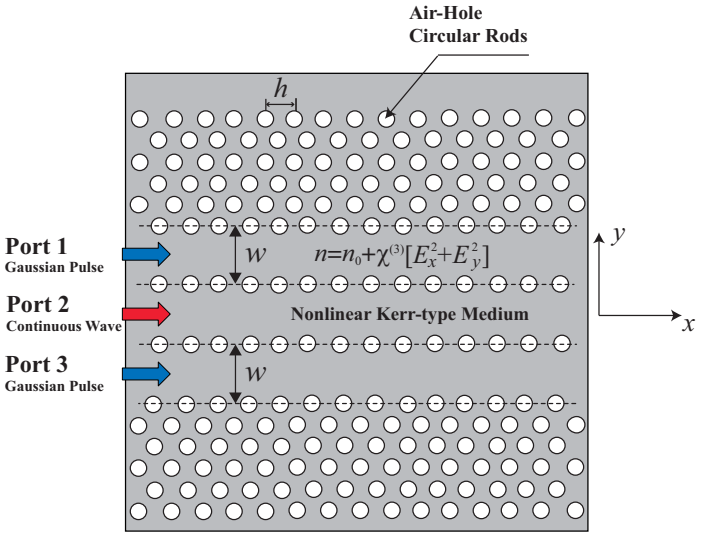

Fig. 1. Schematic view of the three symmetric nonlinear C-PCWs embedded into a planar PhC with a triangular lattice made of air holes in a background nonlinear Kerr-type medium with a linear refractive index $n_0 = 2.95$, where h is the period of the PhC and $w = \sqrt{3}h$ is the width of each of the coupled W1 defect waveguides. The holes are parallel to the z-axis. Number of layers of the upper and lower PhCs is 8. The quantity $\chi^{(3)}$ stands for the third-order nonlinear optical susceptibility of the nonlinear background medium. The length of the photonic crystals is $30h$.

most of the PhC logic gates are operated with continuous wave (CW) signals, whereas this work demonstrates a realistic pulse operation that is very apt for digital signal processing. Solitons maintain a stable pulse envelope along the different C-PCW modules yielding ultrafast full-optical digital signal processing that is characterized only by the peculiarities of the propagation of nonlinear traveling-waves within each gate.

In this manuscript we propose, actually for the first time, the realization of a true all-optical AND logic gate based on the phenomenon of band-gap transmission [11, 12], that could offer a promising scheme for ultra-high throughput optical digital signal processing in the framework of e.g. ultra-fast parity bit checking [13]. A realistic PCW structure, such as the planar air-hole type PhC with a nonlinear silicon background material is studied. Planar silicon PhCs are promising candidates for the successful realization of various nonlinear optical devices on a chip [14–16]. The effect of band-gap transmission takes place when the frequency of the injected signal is very close to the band edge of the PhC. In the linear case no transmission is supposed to occur, whereas in the nonlinear case above some threshold value of the signal amplitude, the propagation of solitons takes place. Such a bifurcation could be observed in both spatial and temporal domains [17]. PhC guarantee a good confinement of the light in the slow light regime, which is a necessary condition for the enhancement of the nonlinear effects [18]. The idea of band-gap transmission was already successfully applied within earlier conceptual studies where we proposed an amplification effect of the signal in both, subwavelength metallic waveguides [19] and coupled PhC waveguides (C-PCWs) [20, 21].

2. Formulation of the problem

The realization of the true all-optical AND logic gate is analyzed based on the three adjacent C-PCWs each consisting of a single line defect (i.e. a W1 waveguide) within a planar PhC with a

Optics EXPRESS

triangular lattice. The cross-sectional view of the structure is shown in Fig. 1. The triangular lattice of air holes is formed in a 2-D nonlinear background dielectric medium where its linear (effective) refractive index is set to $n_0 = 2.95$ in conjunction with a Kerr-type nonlinearity. Here we aim at a typical semiconductor material system (e.g. *Si*, *GaAs*, *InP*) with a relatively high refractive index yielding complete photonic bandgap. In particular in silicon photonics the emergent Kerr-type nonlinearities in bulk c-*Si* are weak and accompanied by strong two-photon absorption (TPA) associated to high free carrier induced loss [22]. For practical application it would be better to use modified material systems with enhanced third order nonlinearities (Kerr-type) based on e.g. amorphous *Si* [23], hybrid organic-*Si*-on-insulator compounds [22, 23], or as possible alternative Ag-polymer based low refractive index PhC slabs with prominent nonlinear optical properties [24].

A number of layers of the upper and lower PhCs is 8 with a lattice constant h and a radius of the air-holes of $r = 0.32h$. The width of each W1 waveguide forming the PCW is $w = \sqrt{3}h$ and the length of the PhC amounts to $30h$. This 2-D model has already proven to be a good approximation of a realistic planar 3-D PCW structure [25, 26], thus enabling a substantial reduction in computation time and what is more important, allows us to reliably demonstrate the realization of true all-optical logic gates. Under the adjusted parameters, the air hole PhC yields a photonic band-gap for the H-polarized field $\left(H_z, E_x, E_y\right)$ covering the frequency range of $0.230 < \omega h/2\pi c < 0.310$, where c is velocity of light and ω is the angular frequency of the excitation. The dispersion diagrams of the three C-PCWs (Fig. 1) are studied based on our original fast rigorous and accurate analysis taking into account the Lattice Sums technique [27] combined with the transition matrix (T-matrix) approach and a recursive algorithm to calculate the generalized reflection and transmission matrices for the PhC [28, 29]. The propagation constant $\beta h/2\pi$ of three C-PCWs (cf. Fig. 1) for both the symmetric (Φ_{S1} and Φ_{S2}) and antisymmetric Φ_A modes versus the normalized frequency is calculated and plotted in Fig. 2 by blue, green and red lines, respectively. The schematic distributions of the magnetic field for the symmetric and antisymmetric modes are presented within the corresponding insets. The dispersion diagrams are plotted only in the normalized frequency range $0.230 < \omega h/2\pi c < 0.270$, since only this region is eligible for the realization of all-optical logic gates. Note that within this region there exist only two symmetric modes and one antisymmetric mode, which are formed by splitting the fundamental mode of the single W1 PCW due to coupling with the adjacent PCWs.

The underlying principle for the realization of the true all-optical logic AND gate - please note that a similar analysis can be applied to realization of OR all-optical logic gate - in the nonlinear C-PCW is as follows: first, we properly choose the operating frequency ω located at the edge of the dispersion curve where no propagating modes are excited (cf. red circle in Fig. 2). At this frequency a continuous signal with amplitude $2A$ is launched into Port 2. The input signal excites the combination of both symmetric modes $A\left(\Phi_{S1} + \Phi_{S2}\right)$. Note that in the linear regime (i.e. small amplitudes of the CW signal) no waves will propagate inside the bulk PhC. Increasing the amplitude of the signal, its frequency acquires a nonlinear shift. Particularly, the dispersion diagram is shifted to the lower frequencies and crosses the black horizontal line (see Fig. 2). As a result, a band-gap transmission of one of the symmetric modes (blue line) occurs and it starts to propagate in the nonlinear C-PCWs. Other two modes are not propagating. The threshold amplitude could be calculated from the relation [12, 21]:

$$\omega = \omega_{S1}(\beta = \pi/h) - \gamma A_{th}^2/4, \tag{1}$$

where $\gamma = 3\omega\chi^{(3)}\kappa/4$, the quantity $\chi^{(3)}$ stands for the third-order nonlinear optical susceptibility and includes an enhancement effect due to the pulse slowdown in the coupled PCWs [18]. Its enhancement is accounted for by multiplying $\chi^{(3)}$ with the square of the slowdown factor - in our case slowdown factor is equal to 16. The coefficient κ takes into account the weakening of the nonlinearity due to the existence of air holes in the planar background material [21]. If we

Optics EXPRESS

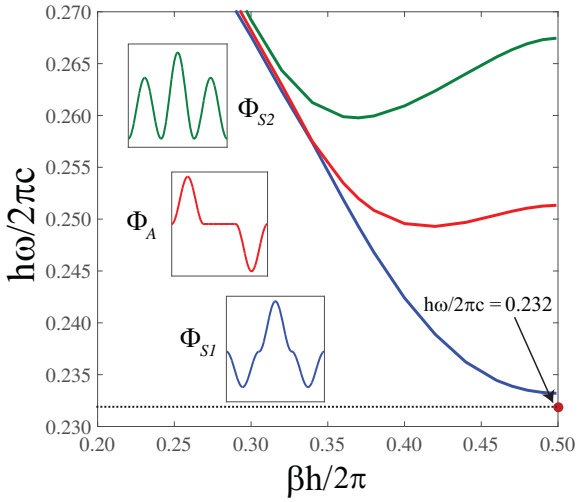

Fig. 2. Dispersion curves of the symmetric (blue and green lines) and the antisymmetric (red line) (super-) modes for the H-polarized field (H_z, E_x, E_y) of the three C-PCWs as shown in Fig. 1. The normalized operation frequency is $\omega h/2\pi c = 0.232$ marked by the red dot. The distributions of the transversal magnetic field H_z for two symmetric (blue and green lines) and one antisymmetric (red line) modes are shown in the corresponding insets.

properly choose the amplitude of the CW signal to be below the threshold amplitude A_{th} for band-gap transmission, no waves will propagate inside the nonlinear C-PCWs. Next, a Gaussian signal pulse (i.e. a carrier signal with Gaussian pulse envelope) with amplitude δ injected into the upper and/or the lower waveguide of the three C-PCWs can now trigger the band-gap transmission process.

Formally, this results in the excitation of a combination of modes according to $\sqrt{2}\delta\left(\Phi_{S1} - \Phi_{S2} + 2\Phi_A/\sqrt{2}\right)/4$ that enhances the amplitude of the symmetric mode Φ_{S1} reaching the condition that allows for band-gap transmission whereas the other modes remain evanescent. Hence, the input pulse will be carried by the only propagating symmetric mode Φ_{S1} that has now formed a propagating soliton inside the C-PCW structure with the shape given as:

$$H_z(x, y, t) = F\frac{\Phi_{S1}(x, y)\exp(i\delta\omega t)}{\cosh\left[(x - v_{S1}t)/\Lambda\right]}e^{i(\beta x - \omega t)} + c.c. \tag{2}$$

Here F is a soliton amplitude, Λ is a soliton width, $\delta\omega$ denotes the frequency shift of the localized modes due to the nonlinearity of the background material and v_{S1} denotes the group velocity for symmetric mode Φ_{S1}. It is worth noting that knowing the excitation frequency ω and the amplitude F of the soliton, we can define the propagation constant β using the relation $\omega = \omega_{S1}(\beta) - \gamma F^2/4$, whereas the other parameters, such as the soliton width Λ, the group velocity v_{S1} and the frequency shift $\delta\omega$ are given as follows:

$$\Lambda = \sqrt{\frac{2\omega''_{S1}}{\gamma F^2}},\quad \omega''_{S1} = \frac{\partial^2\omega_{S1}}{\partial\beta^2},\quad v_{S1} = \frac{\partial\omega_{S1}}{\partial\beta},\quad \delta\omega = \frac{\gamma F^2}{4}. \tag{3}$$

Key to the realization of true all-optical logic gates is perfect "digitalization" in the process of band-gap transmission. This means that, when operating frequency of the CW signal launched in Port 2 is located sufficiently close to the photonic band edge, the weak signals injected into

Optics EXPRESS

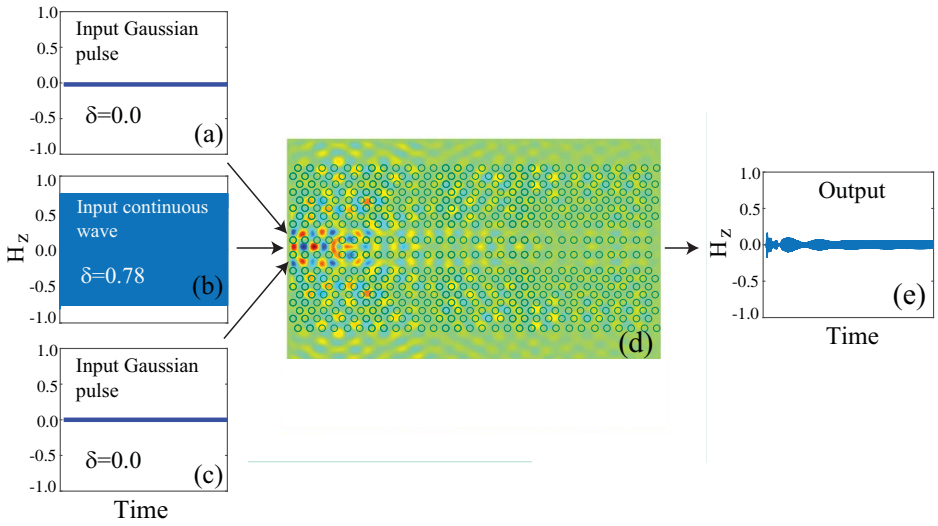

Fig. 3. Schematic distributions (H_z) of the signal pulses propagating (d) inside the nonlinear C-PCWs (Fig. 1), when a CW input signal with the amplitude $\delta = 0.78$ is launched through Port 2 and no input signals $\delta = 0$ are injected into Port 1 (a) and Port 3 (c). Magnetic field H_z of the received signal at a distance $x = 30h$ inside the C-PCW associated to Port 2 (e).

Port 1 and/or Port 3 are becoming capable to overcome the amplitude threshold and a soliton can be generated with amplitude and shape that is completely defined by the CW signal injected into Port 2. In other words, the weak input pulse just triggers the creation of a stable soliton with predefined amplitude yielding a complete regeneration of the input signal pulse prior (and during) the proposed optical digital signal processing [21,30,31]. Note that within the context of the aforementioned "digitalization" Port 2 can be viewed as an "enable pin" of the proposed logic gate where the CW signal will act as the "enable signal" common in digital electronics.

3. Numerical results and discussions

For a reliable proof of concept comprehensive full-wave computational electromagnetics analyses are conducted based on the finite-difference time-domain (FDTD) method using the Berenger's PML to confine the simulation domain [14,32] at the fixed normalized frequency $\omega h/2\pi c = 0.232$ marked by the red dot in Fig. 2. It should be emphasized that the frequency is located at the edge of the dispersion curve of the symmetric mode (blue line). Figures 3-5 illustrate the subsequent realization of an operational all-optical AND gate. First, a CW signal, whose transversal electric field is in plane to the planar PhC, with the normalized operation frequency $\omega h/2\pi c = 0.232$ and an amplitude of $\delta = 0.78$ is launched into Port 2 of C-PCW structure [cf. Fig. 3(b)], whereas no signal $\delta = 0$ is launched into Port 1 [Fig. 3(a)] and Port 3 [Fig. 3(c)]. The peak power of the injected signal pulses is chosen as $\chi^{(3)}E_0^2 = 0.08$, where $E_0 = \sqrt{(E_x^0)^2 + (E_y^0)^2} = \delta\sqrt{\mu_0/\epsilon_0 n_0^2}$ is the electric field amplitude of the CW signal launched into Port 2 of C-PCW structure. Figure 3(d) depicts the distributions of the propagating soliton inside the nonlinear C-PCWs. The output signal is registered at a distance $x = 30h$ at the end of the C-PCWs where the magnetic field H_z is depicted in Fig. 3(e). Since the amplitude of the CW is below the threshold, no soliton is generated and the amplitude of the output signal is almost zero. Next, we additionally inject a Gaussian pulse into Port 1 at the same normalized frequency $\omega h/2\pi c = 0.232$ with an amplitude $\delta = 0.72$ as it is shown in Fig. 4(a), whereas no signal is injected in Port 3. The full width at half maximum pulse duration is $800h/c$ corresponding to values around 1.0-1.2 ps for typical

Optics EXPRESS

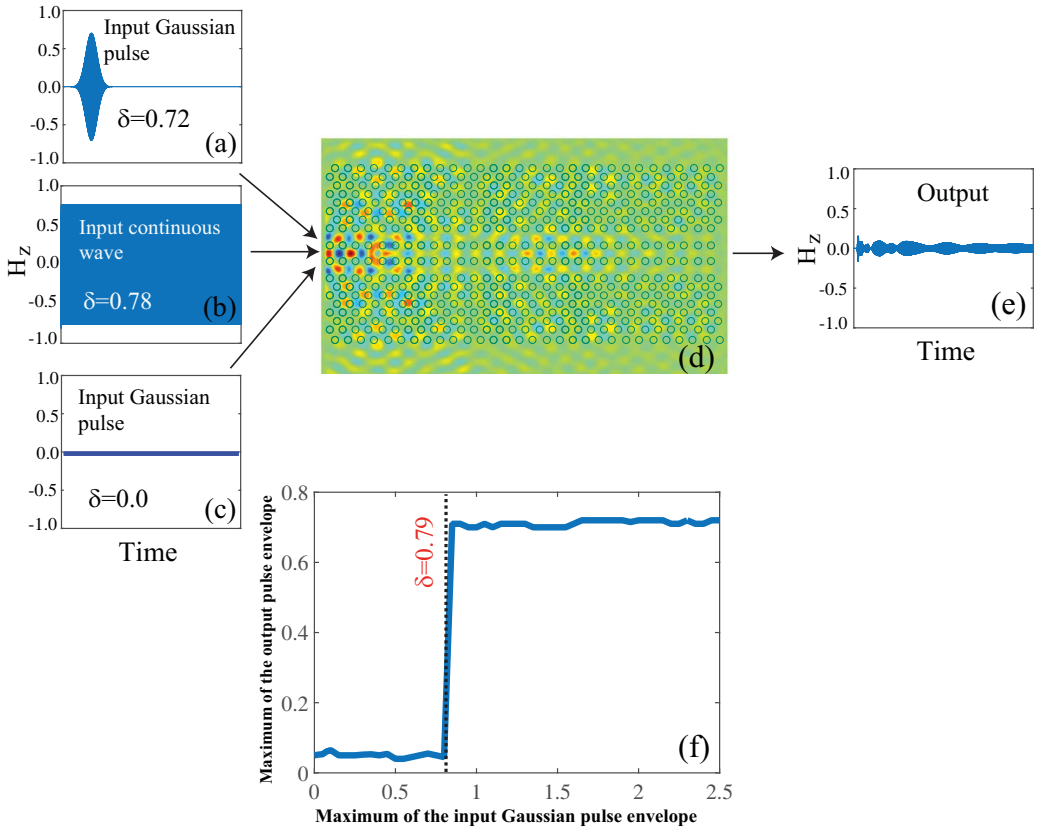

Fig. 4. Schematic distributions (H_z) of the signal pulses propagating (d) inside the nonlinear C-PCWs (Fig. 1), when a CW signal with the amplitude $\delta = 0.78$ is launched through Port 2 (b), and a Gaussian pulse with amplitude $\delta = 0.72$ is injected into Port 1(a), whereas no single is injected into Port 3 (c). Magnetic field H_z of the received signal at a distance $x = 30h$ inside the C-PCW associated to Port 2 (e). Amplitude transfer curve, which represents the dependence of the maximum of the output pulse envelope versus the maximum of the input Gaussian pulse envelope injected in Port 1 (f).

lattice constants. An increased input power compared to Fig. 3 causes the dispersion $\omega(\beta)$ to shift to lower frequencies because of the underlying Kerr-type nonlinearity, however it cannot overcome the threshold value to reach an operation point that allows for a propagating soliton inside the C-PCW. Hence, the registered output signal at the end of the C-PCW is almost zero as displayed in Fig. 4(e). Figure 4(f) depicts the amplitude transfer curve illustrating the dependence of the maximum of the output pulse envelope versus the maximum of the input Gaussian pulse envelope injected in Port 1 given no input signal at Port 3. The transfer curve shows a very distinct transition at $\delta = 0.79$, meaning that above this value any single input pulse will cause an optical output pulse as the input signal starts propagating inside the C-PCWs due to the nonlinearity of the background medium. In order to realize functional all-optical AND logic gate, the injected Gaussian pulse (e.g. in Port 1) should therefore be smaller than $\delta = 0.79$. Another point worth mentioning is that the maximum of the output pulse envelope barely depends on the maximum of the input Gaussian pulse envelope. This unique feature of the band-gap transmission phenomenon is used in Fig.5, when we simultaneously inject an additional signal pulse into Port 3 (which is in phase to the signal injected in Port 1). Due to the interference of the pulses, the threshold

Optics EXPRESS

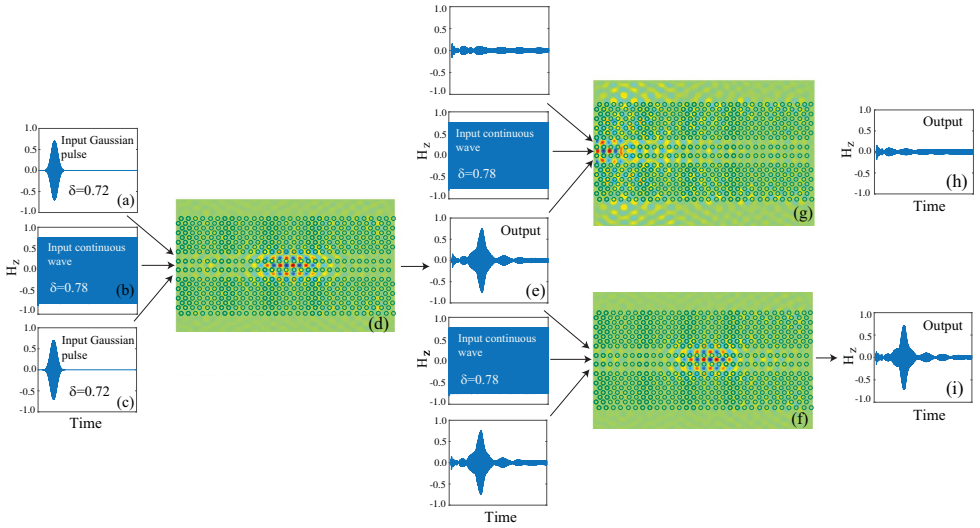

Fig. 5. Schematic distributions (H_z) of the signal pulses propagating (d) inside the nonlinear C-PCWs (Fig. 1), when a CW signal with the amplitude $\delta = 0.78$ is launched through Port 2 and Gaussian pulses with an amplitude $\delta = 0.72$ are injected into Port 1 and Port 3. Magnetic field H_z of the received signal at a distance $x = 30h$ inside the C-PCW associated to Port 2 (e). Schematic distributions (H_z) of the signal pulses propagating (f) inside the nonlinear C-PCWs (Fig. 1), when a CW input signal with the amplitude $\delta = 0.78$ is launched through Port 2 and the output signal (e) is injected as a new input signal into Port 1 and Port 3 of a subsequent C-PCW stage. Magnetic field H_z of the received signal at a distance $x = 30h$ inside the C-PCW associated to Port 2 (i). Schematic distributions (H_z) of the signal pulses propagating (g) inside the nonlinear C-PCWs (Fig. 1), when a CW input signal with the amplitude $\delta = 0.78$ is launched through Port 2 and the output signal (e) is injected as a new input signal into Port 3. No single is injected into Port 1 of a subsequent C-PCW stage. Magnetic field H_z of the received signal at a distance $x = 30h$ inside the C-PCW associated to Port 2 (h). The peak level contrast between the "1" and "0" overall output signal amounts to 16 dB.

value is exceeded, a soliton is generated and the characteristics of the output signal pulse at Port 2 (namely its amplitude and width) are very close to those of the input signal pulse showing a relative error about 9% (Fig. 5). The associated bandwidth is estimated to be around 300 GHz. We successively repeat the process and inject the output signal in Fig. 5(e) as a new input signal to the C-PCWs. Hence, the most challenging case, such as cascaded system, is considered. The schematic distributions of the magnetic field inside the guiding system and the resulting output signals are depicted in Figs. 5(f), 5(g) and Figs. 5(i), 5(h), respectively. Note that the output signal pulse shown in Fig. 5(i) is still very similar to those of the original input signal pulses deviating only by a relative error of about 12%. When we further successively repeat the process, the relative error does not show any noticeable change. Hence, the realization of a true all-optical AND logic gate has been vividly demonstrated within a realistic pulse signal operation scenario apt for future digital photonics. In our numerical analysis we assume coherent carriers where the carrier phases of the input Gaussian pulses are approximately in line with the phase of the CW input signal. However, the proposed scheme even works for minor phase deviations (i.e. partially in phase). Regarding the timing mismatch of the involved pulse envelopes the proposed scheme is still operational when the time differences between the Gaussian amount to 0.3 - 0.4 ps for typical lattice constants. The latter will only affect the time of the soliton formation.

Finally, we briefly mention about the backscattering loss. Backscattering and waveguide

Optics EXPRESS

losses have been investigated using full-wave computational electromagnetic simulations as well as corresponding reflection/transmission measurements in [33]. It has been shown that a backscattering is virtually negligible in the bandgap region. At the band edges, there exists backscattering loss, which exponentially decreases towards the bandgap region.

4. Conclusion

In conclusion it is worth emphasizing that based on the phenomenon of band-gap transmission we have proposed a functional true AND all-optical logic gate (1) using a realistic model of a coupled Kerr-type nonlinear air-hole type C-PCWs, and (2) that is operating with realistic optical signal pulses. Our numerical analyses have shown that even for the most challenging case, such as cascaded systems yielding all-optical multiple-input logic gates, the shape of the output signal (namely its amplitudes and associated widths) is in a very close agreement with those for the original input signal. Each C-PCW module underlying the logic gate is yet capable to provide all-optical regeneration (2R: reamplification and re-shaping) for signal pulses above the aforementioned threshold for soliton propagation. It is important to mention that our analysis can be also applied to realize the true all-optical multiple-input OR gate in a similar a cascaded topology. However, some modifications are needed, because the time for soliton formation when injecting the Gaussian pulses either into Port 1 or Port 3 is slightly different compared to the case where the Gaussian pulses are simultaneously injected into Port 1 and Port 3. Hence, proper timing issues are now under intense investigation.

Funding

Shota Rustaveli National Science Foundation (SRNSF) (Grants Nos 216662, FR/25/6-100/14 and STCU-2016-03); Science and Technology Center in Ukraine (grant No 6303); Alexander von Humboldt Foundation; Joint travel grant from Georgian SRNSF and CNRS France (grant No 04/01).